Electrical Properties of α-Ga_2O_3 films grown by Halide Vapor Phase Epitaxy on sapphire with α-Cr_2O_3 buffers

Alexander Polyakov[1], Vladimir Nikolaev[2,3], Sergey Stepanov [3], Alexei Almaev [4], Alexei Pechnikov [2,3], Eugene Yakimov[1, 5], Bogdan O. Kushnarev[4], Ivan Shchemerov[1], Mikhail Scheglov[2], Alexey Chernykh[1], Anton Vasilev[1], Anastasia Kochkova[1] and Stephen J. Pearton[6]

[1]National University of Science and Technology MISiS, 4 Leninsky Avenue, Moscow 119049, Russia

[2]Ioffe Institute, 26 Politekhnicheskaya, Saint Petersburg, 194021, Russia

[3] Perfect Crystals LLC, 28 Politekhnicheskaya, Saint Petersburg, 194064, Russia

[4]Tomsk State University, 36 Lenin Avenue, Tomsk, 634050, Russia

[5]Institute of Microelectronics Technology RAS, Chernogolovka 142432, Russia

[6]Department of Materials Science and Engineering, University of Florida, Gainesville, FL 32611, USA

ABSTRACT

We report on growth and electrical properties of α-Ga_2O_3 films prepared by Halide Vapor Phase Epitaxy (HVPE) at 500ºC on α-Cr_2O_3 buffers predeposited on sapphire by magnetron sputtering. The α-Cr_2O_3 buffers showed a wide MCL peak near 350 nm corresponding to the α-Cr_2O_3 bandgap and a sharp MCL line near 700 nm due to the Cr^+ intracenter transition. Ohmic contacts to Cr_2O_3 were made with both Ti/Au or Ni, producing linear current-voltage (I-V) characteristics over a wide temperature range with an activation energy of conductivity of ~ 75 meV. The sign of thermoelectric power indicated p-type conductivity of the buffers. Sn-doped, 2-μm-thick α-Ga_2O_3 films prepared on this buffer by HVPE showed donor ionization energies 0.2-0.25 eV while undoped films were resistive with the Fermi level pinned at E_C-0.3 eV. The I-V and capacitance-voltage (C-V) characteristics of Ni Schottky diodes on Sn-doped samples using a Cr_2O_3 buffer indicated the presence of two face-to-face junctions, one between n-Ga_2O_3

and p-Cr_2O_3, the other due to the Ni Schottky diode with n-Ga_2O_3. The spectral dependence of the photocurrent measured on the structure showed the presence of three major deep traps with optical ionization thresholds near 1.3 eV, 2 eV, and 2.8 eV. Photoinduced Current Transient Spectroscopy (PICTS) spectra of the structures were dominated by deep traps with ionization energy of 0.95 eV. These experiments suggest another pathway to obtaining p-n heterojunctions in the α-Ga_2O_3 system.

Journal of Applied Physics

AIP Publishing

I. INTRODUCTION

Ga_2O_3 is a next generation wide bandgap semiconductor for high-power electronic devices and solar-blind photodetectors [1-11]. The main thrust of research in this material system has understandably been on the thermally stable monoclinic β-Ga_2O_3 polymorph, for which high crystalline quality large diameter single crystals can be prepared from the melt and used as native substrates for growth of β-Ga_2O_3 epitaxial films by Halide Vapor Phase Epitaxy (HVPE), Metalorganic Chemical Vapor Deposition (MOCVD), Molecular Beam Epitaxy (MBE), while heterojunctions with a wider-bandgap ternary $(Al_xGa_{1-x})_2O_3/Ga_2O_3$ can be prepared by MBE or Pulsed Laser Deposition (PLD) and used for fabrication of Modulation Doped Field Effect Transistor (MODFET) structures [1,3,4-10]. These studies have resulted in demonstrations of power rectifiers, MODFETs, transistors and UV photodetectors with attractive performance [1-8,10,11].

In addition, the properties of metastable corundum α-Ga_2O_3 have also created great interest recently due to an even larger bandgap than for α-Ga_2O_3 (5.3 eV versus 4.8 eV) [9], the possibility to perform the growth on very robust and mature isomorphous sapphire (α-Al_2O_3) substrates and the existence of a host of corundum-structured rare earth or transition metal oxides with a natural p-type conductivity, which makes it possible to prepare n-p heterojunctions and solid solutions with p-type conductivity [9, 12-28]. The latter consideration is of particular importance because of the well known lack of suitable p-type dopants with low ionization energy in Ga_2O_3 films or crystals of any polytype and the strong tendency of holes to form self-trapped hole polaronic states [5,6]. This is due to the very deep valence band position with respect to the vacuum level, the strong ionic contribution to bonding, strong electron-phonon coupling, and the very flat valence band formed by oxygen p-states [29,30]. Hybridization with the d-states of the partly filled d-shell of Ir in α-$(Ir_xGa_{1-x})_2O_3$ can considerably lift the top of the valence band and make it possible to obtain natural vacancy-related p-type conductivity that can be strongly enhanced by Mg doping, while preserving the attractively high bandgap of 4.3 eV [27,28, 31].

Similar effects can be expected for other transparent metal oxides comprising transition metals [8]. Thus, combining α-Ga_2O_3 with α-Cr_2O_3 could be of interest because of the higher bandgap of Cr_2O_3 compared to Ir_2O_3 and a close lattice match between the α-Ga_2O_3 and the α-Cr_2O_3, presumably conducive to good solubility of components over the entire composition range [8]. We have already demonstrated that HVPE growth of α-Ga_2O_3 films on basal plane sapphire with pre-deposited thin α-Cr_2O_3 buffers prepared by magnetron sputtering and annealing decreases the overall threading dislocation density in Ga_2O_3 by a factor of 4 times, from 2×10^{10} cm^{-2} to 5×10^{9} cm^{-2}, because of the improved relief of strain caused by the lattice mismatch between sapphire and Ga_2O_3[32].

In this paper, we describe the effects of introducing such Cr_2O_3 buffer layers on electrical properties and deep trap spectra of α-Ga_2O_3 films. The buffer layers are found to be p-type from thermopower measurements due to 75 meV acceptors, while the α-Ga_2O_3 is found to be insulating when undoped and n-type when doped with Sn. In PICTS, a prominent feature in samples with the Cr_2O_3 underlayers was the dominance of traps with ionization energy at 0.95 eV as opposed to the 0.35 eV traps in samples without the underlayer.

II.EXPERIMENTAL

The Cr_2O_3 films used were deposited in an RF magnetron sputtering system (A-500 Edwards, UK). C-plane sapphire wafers of 330 - 440 μm thickness and 50 mm in diameter were used as substrates. Before deposition, the sapphire substrates were cleaned in sulfuric acid and isopropanol. A 99.95% chromium target and oxygen-argon plasma were used as source materials. The concentration of oxygen in the plasma was 56.1 ± 0.5 vol.%. The distance between the substrate and the target was 70 mm. The deposition was carried out at a working pressure of $7x10^{-3}$ mbar and RF power of 70 W. The temperature of the substrate was not controlled during the sputtering. The deposition was carried out for 45 minutes to reach a thickness of about 150 nm, but some structures were made thicker, 400 nm, for electrical characterization. After deposition, the Cr_2O_3 films were annealed in air at 500 °C for 3 hours. As-

deposited Cr_2O_3 films were microcrystalline textures with preferred orientation (0001) and microcrystal dimensions of around 50 nm. Annealing for 3 hours at 500°C led to a certain ripening of the grains in the texture and increase of their dimensions to about 100 nm.

Ga_2O_3 films were grown in a homemade atmospheric horizontal quartz HVPE reactor. Gallium chloride (GaCl) and oxygen (O_2) were used as precursors. GaCl was synthesized *in situ* by passing gaseous hydrogen chloride (HCl, 99.999% pure) over metallic gallium (Ga, 99.9999% pure) at 600°C. The GaCl and O_2 were then mixed in the deposition zone of the reactor to produce Ga_2O_3 on the substrate. Argon was used as a carrier gas to keep the total gas flow rate through the reactor at 10 slm. The deposition temperature was 500°C. The VI/III (O_2/GaCl) ratio was 4.2. Under these conditions, the growth rate was 2.4 μm/h. To ensure identical growth conditions and fair comparison, the growth on sapphire substrates with and without Cr_2O_3 buffer was conducted in the same growth run. The grown films with and without the Cr_2O_3 buffer were doped with Sn via introducing the volatile Sn salt in one of the channels of our HVPE machine. In these experiments first about 2 μm of undoped film were grown and then the top ~1 μm of the film was doped with Sn.

The phase composition of the produced films was investigated by x-ray diffraction (XRD) analysis using $CuK_{\alpha 1}$ radiation. The structural quality of the films was estimated from the full width at half maximum (FWHM) of XRD rocking curves (RC) of symmetric (0006) and skew-symmetric (10-18) reflections of α-Ga_2O_3.

For electrical characterization of the Cr_2O_3 and Ga_2O_3 films, Ti/Au contacts (20nm/ 80 nm) and Ni contacts were deposited by e-beam evaporation through a shadow mask. The Ti/Au contacts of 1 mm in diameter and 2 mm pitch were subjected to rapid thermal annealing at 300°C in nitrogen for 2 minutes to form Ohmic contacts. Circular Ni contacts (20 nm thick) were deposited at room temperature to act as semi-transparent Schottky diodes [33-36]. Electrical characterization involved current-voltage (I-V) measurements between the Ohmic Ti/Au contacts

and between the Ni and Ti/Au contacts. These measurements were done in the dark and under illumination with a set of visible-near-UV Light Emitting Diodes (LEDs) with wavelengths between 940 nm and 365 nm and output power up to 1 W (the actual spectral measurements were done with the output power density of 250 mW/cm^2). The photocurrent measurements in the near-bandedge region were done with 259 nm UV LEDs at an output power density of 1.2 mW/cm^2. For samples showing good rectification for Ni Schottky diodes, capacitance- frequency (C-f), capacitance-voltage (C-V) measurements were performed in the frequency range 20 Hz-20 MHz in the dark and under monochromatic illumination.

The deep trap spectra of the samples were obtained from admittance spectroscopy (AS) [37] and from Photinduced Current Transient Spectroscopy (PICTS) [36] because standard Deep Level Transient Spectroscopy (DLTS) was not applicable for our samples with high series resistance. These measurements were performed from 77K to 500K using a liquid nitrogen cryostat (Cryotrade Instruments, Russia) [33-39]. The optical charaterization of the grown films was done by Microcathodoluminescence (MCL) spectra measurements at 300K and 90K[33, 36].

III.RESULTS AND DISCUSSION

III.1. Electrical and optical properties of the Cr_2O_3 films.

Detailed measurements were performed for the Cr_2O_3 films deposited on basal plane sapphire and subjected to 3 h annealing in air at 500ºC. The thickness of these films was 0.4 μm. The Ti/Au contacts I-V characteristics were linear at all temperatures and the films showed photosensitivity for above-bandgap excitation at 364 nm wavelength, as shown in Figure 1. Ni contacts showed no rectification and their properties were not different from the Ohmic Ti/Au contacts. Thermal probing of the Cr_2O_3 films showed the material was p-type, but Hall/van der Pauw and C-V measurements were not possible because of the low magnitude of the Hall signal.

The temperature dependence of the current through the Ohmic contacts showed an activation energy of 75 meV (Figure 2) which likely corresponds to the depth of the native acceptors in the film. The room temperature MCL spectrum of the Cr_2O_3 layer is shown in

Figure 3 and consisted of a broad band peaked near 349 nm and a sharp line at 694 nm. The broad peak corresponds to bandedge luminescence with bandgap ~ 3.5 eV. The sharp line is most likely related to the intracenter transition in the Cr ion [40]. Overall, the electrical and optical properties of our Cr_2O_3 films are in agreement with previously published results which ascribed the acceptors dominating the resistivity of the films to Cr vacancies [41,42].

III.2. Ga_2O_3 films grown on basal plane sapphire with and without Cr_2O_3 buffer annealed at 500°C.

For the films grown with moderate Sn doping, Figure 4 shows the room temperature C-f characteristics of the two types of films. The C-f characteristic of the layer without the Cr_2O_3 buffer displays a low-frequency plateau extending to ~1 kHz, corresponding to deeper donors, another poorly resolved plateau near 10 kHz related to shallower donors, and a sharp drop after 10 kHz due to the series resistance of the diode. Admittance spectra indicated the shallow donors had ionization energy 0.2-0.25 eV, while there were also deeper centers at 0.3-0.35 eV. $1/C^2$ versus voltage V plots showed clearly the linear dependence due to the doped portion of the film and a plateau, once the space charge region boundary is swept through the doped portion and reaches the relatively highly resistive portion. Electrical measurements on a similarly grown sample with no top Sn doped region showed that in undoped films the Fermi level is pinned near E_c-0.3 eV, as shown in Figure 5(a). The charged centers concentration profiles calculated from low-frequency (300 Hz) and high-frequency (3 kHz) C-V data are shown in Figure 6. According to the C-f and admittance spectra measurements, the low-frequency profile corresponds to the total density of the shallow and deep donors, while the high-frequency profile only gives the depth distribution of the shallow donors [37].

The total density of the shallow and deep donors deduced from the 300 Hz profile was 8×10^{15} cm^{-3} near the surface, leveled off between 0.5-0.7 μm at 3×10^{15} cm^{-3}, and then decreased as the space charge region (SCR) boundary approached the edge of the intentionally Sn doped portion of the film. Measurements at 3 kHz yielding the profile of the shallow donors coincided

with the low frequency profile at depths from the surface exceeding 0.6 μm, indicating that for these depths, the shallow donors dominate. Their concentration gradually decreased to below 2×10^{15} cm^{-3} near 0.9 μm, approximately where the Sn doping was initiated during growth. Thus, it seems fair to state that, in the near-surface regions, the dominant donor species are the 0.35 eV donors, whereas, for deeper regions, the dominant species are the 0.25 eV donors. This is in line with our earlier observations for lightly doped α-Ga_2O_3 films [36] and points to a complex nature of donors rather than just simple substitutional Sn centers. [36].

For the sample grown on Cr_2O_3 buffer, the low frequency plateau below 1 kHz was not observed, the capacitance showed a poorly defined plateau near 1 kHz and fell off totally for frequencies above 10 kHz because of the high series resistance (Figure 4). $1/C^2$ versus V plots were unusual in that they displayed a plateau at forward biases and low reverse biases, with the slope of the plot for high reverse voltages implying p-type conductivity (Figure 5(b)).

The current-voltage I-V characteristics of the two types of diodes were also radically different, as illustrated in Figure 7(a, b). For the sample without the Cr_2O_3 buffer the I-V characteristic was of the normal type expected for a Schottky diode on n-type film (i.e. the current for positive voltage applied to the Ni Schottky contact was much higher than at negative voltage). In contrast, the I-V characteristic of the samples with Cr_2O_3 buffer was quite unusual. The current in the forward direction was actually lower than the current in reverse direction. This was not a consequence of non-ideality of the Ohmic contacts as the I-V dependence measured between the two Ohmic contacts was linear (Figure 8). The behavior under illumination was also totally different for the two types of samples. For samples without the Cr_2O_3 buffer, illumination with sub-bandgap light caused an increase of photocurrent in reverse direction only for high optical power density and was, as usual, related to electron excitation from deep traps in the bandgap. Above-bandgap illumination with a 259-nm-wavelength LED created a high photocurrent even for optical power densities ~100 times lower than for the sub-bandgap light because of effective generation of electrons and holes. Both types of excitations caused only

slight changes in the forward current branch and the series resistance of the Ga_2O_3 film (Figure 7(a)). By contrast, for the samples with Cr_2O_3 buffer, the photocurrent was equally high in both directions (Figure 7(b)).

A quantitative model explaining the differences in behavior of the two types of samples has not been developed yet, but it seems very likely that the existence of the parasitic p-Cr_2O_3/n-Ga_2O_3 heterojunction could be responsible for the observed phenomena in C-V and I-V data in the dark and under monochromatic illumination. Some additional insight is provided by photocapacitance spectra, photocurrent spectra, and PICTS measurements. The photocapacitance spectra displayed in Figure 9 are quite similar for both samples and show three distinct optical thresholds, one near 2 eV, second near 2.8 eV, and third near 3.1 eV.

In photocurrent spectra of the sample without the Cr_2O_3 underlayer, significant changes were observed only at reverse voltages and low forward voltages. Figure 10 (a) displays the data for reverse voltage -4V. The spectrum is similar to the photocapacitance spectrum, with two prominent thresholds at 2.8 eV and 3.1 eV. For the sample with the Cr_2O_3 buffer, the photocurrent spectra are shown for reverse voltage of -1V (the plateau in I-V characteristics) and for forward voltage of 5V (approximate saturation in photocurrent). The data show optical thresholds near 1.3 eV (specific for I-V spectra, not clearly observed in photocapacitance) and 2 eV (similar to photocapacitance), with no prominent features at higher energies.

PICTS spectra of the two samples are compared in Figure 11. For the sample without the Cr_2O_3 buffer, the PICTS spectra were dominated by deep centers with ionization energy 0.35 eV while in the samples with Cr_2O_3 buffer, the spectra were dominated by the peak belonging to the trap with ionization energy of 0.95 eV. The features observed in the photocapacitance spectra, photocurrent spectra, and PICTS spectra of the Ga_2O_3 films without the Cr_2O_3 buffer are rather common for our α-Ga_2O_3 films. For the epilayers grown on the Cr_2O_3 buffers, the distinguishing characteristics are higher dark current in reverse direction than in the forward direction, the presence of a prominent plateau in reverse direction at low reverse voltage, the strong

photosensitivity in the forward direction, in contrast to the sample without the underlayer, and the presence in photocurrent spectra of an additional optical threshold near 1.3 eV and the lack of optical thresholds near 2.8 eV and 3.1 eV observed in the reference sample. In PICTS the prominent feature in the sample with the Cr_2O_3 underlayer was the dominance of traps with ionization energy at 0.95 eV as opposed to the 0.35 eV traps in the samples without the underlayer.

SUMMARY and CONCLUSIONS

Growth of α-Ga_2O_3 films on α-Cr_2O_3 buffer deposited by magnetron sputtering and annealed at 500^{o}C leads to a factor of 4 decrease of the threading dislocation density and can provide a p-n junction capability. The Cr_2O_3 films are p-type according to thermal probing, with the acceptors having an ionization energy of 75 meV as determined from the temperature dependence of current between the Ohmic contacts. MCL spectra were dominated by a broad bandedge peak near 350 nm and a sharp peak at 700 nm peak due to intracenter transitions in the Cr^+ ion. The presence of this p-type layer manifests itself in several unusual features in C-V and I-V characteristics measured in the dark and under monochromatic illumination with peak wavelengths ranging from 365-940 nm. In C-V characteristics, the dark capacitance is independent of voltage at forward and low reverse voltages while, for high reverse voltages, it demonstrates p-type-like behavior. In I-V characteristics, the dark current is higher at reverse voltage than at forward voltage, the photocurrent in the forward direction is higher than in reverse direction. In PICTS spectra, the dominant peak belongs to centers with ionization energy 0.95 eV for the samples with Cr_2O_3 underlayer rather than 0.35 eV for the samples without this underlayer.

Further studies involving heavier n-type doping of the films, growth on nonpolar or semi-polar orientations are needed to better understand the effects of Cr_2O_3 buffers on changing the threading dislocation density and the type and density of electron and hole traps. Our data suggests that using ternary solid solutions of α-$(Cr_xGa_{1-x})_2O_3$ could be instrumental in obtaining

p-type films with a very wide bandgap, similarly to the case of $(Ir_xGa_{1-x})_2O_3$ [31]. Ternary solutions with Cr_2O_3 potentially offer better performance because of a very good lattice matching between α-Ga_2O_3 and α-Cr_2O_3, and wider bandgap of Cr_2O_3 than Ir_2O_3, both facilitating a high solubility in the entire composition range, a relative ease in obtaining low interface states density between the p-type ternaries and the n-type Ga_2O_3 and a higher bandgap of the solid solutions with feasible p-type doping.

Conflict of interest

The authors have no conflicts to disclose

DATA AVAILABILITY

All data that support the findings of this study are included within the article.

ACKNOWLEDGMENTS

The work at NUST MISiS was supported in part by the Russian Science Foundation, grant no. 19-19-00409. The work was performed as part of Interaction of Ionizing Radiation with Matter University Research Alliance (IIRM-URA), sponsored by the Department of the Defense, Defense Threat Reduction Agency under award HDTRA1-20-2-0002. The content of the information does not necessarily reflect the position or the policy of the federal government, and no official endorsement should be inferred. The work was also supported by NSF DMR 1856662.

REFERENCES

1. S. J. Pearton, Fan Ren, Marko Tadjer, and Jihyun Kim, J. Appl. Phys. 124, 220901 (2018).
2. J. Xu, W. Zheng and F. Huang, J. Mater. Chem. C, 7, 8753 (2019).
3. Damanpreet Kaur and Mukesh Kumar, Adv. Optical Mater.9, 2002160 (2021).
4. Man Hoi Wong and Masataka Higashiwaki, IEEE Trans. Electron. Dev. 67, 3925 (2020).
5. Gallium Oxide: Materials Properties, Crystal Growth, and Devices, ed. Masataka Higashiwaki and Shizuo Fujita (Springer Series in Materials Science ISBN 978-3-030-37152-4 ISBN 978-3-030-37153-1, 2020) parts 1-3
6. Gallium Oxide: Materials Properties, Crystal Growth, and Devices, ed. Masataka Higashiwaki and Shizuo Fujita (Springer Series in Materials Science ISBN 978-3-030-37152-4 ISBN 978-3-030-37153-1, 2020), part 4
7. Andrew J. Green, James Speck, Grace Xing, Peter Moens, Fredrik Allerstam, Krister Gumaelius, Thomas Neyer, Andrea Arias-Purdue, Vivek Mehrotra, Akito Kuramata, Kohei Sasaki, Shinya Watanabe, Kimiyoshi Koshi, John Blevins, Oliver Bierwagen, Sriram Krishnamoorthy, Kevin Leedy, Aaron R. Arehart, Adam T. Neal, Shin Mou, Steven A. Ringel, Avinash Kumar, Ankit Sharma, Krishnendu Ghosh, Uttam Singisetti, Wenshen Li, Kelson Chabak, Kyle Liddy, Ahmad Islam, Siddharth Rajan, Samuel Graham, Sukwon Choi, Zhe Cheng, and Masataka Higashiwaki, APL Mater. 10, 029201 (2022).
8. Kentaro Kaneko, Shizuo Fujita, and Toshimi Hitora, Jpn. J. Appl. Phys 57, 02CB18 (2018).
9. Elaheh Ahmadi and Yuichi Oshima, J. Appl. Phys. 126, 160901 (2019).
10. Hongpeng Zhang, Lei Yuan, Xiaoyan Tang, Jichao Hu, Jianwu Sun, Yimen Zhang, Yuming Zhang and Renxu Jia, IEEE Trans. Power Electron. 35, 5157 (2020).

11. Alexander Y. Polyakov, Vladimir I. Nikolaev, Eugene B. Yakimov, Fan Ren, Stephen J. Pearton, and Jihyun Kim, J. Vac. Sci. Technol. A 40, 020804 (2022).
12. I. Cora, Z. Fogarassy, R. Fornari, M. Bosi, A. Recˇnik, and B. Pecz, Acta Mater. 183, 216 (2020).
13. A. U. Bhuiyan, Z. Feng, J. M. Johnson, H.-L. Huang, J. Sarker, M. Zhu, M. R. Karim, B. Mazumder, J. Hwang, and H. Zhao, APL Mater. 8, 031104 (2020).
14. M. Hilfiker, U. Kilic, M. Stokey, R. Jinno, Y. Cho, H. G. Xing, D. Jena, R. Korlacki, and M. Schubert, Appl. Phys. Lett. 119, 092103 (2021).
15. Kazuyuki Uno, Riena Jinno, and Shizuo Fujita, J. Appl. Phys. 131, 090902 (2022).
16. Joseph A. Spencer, Alyssa L. Mock, Alan G. Jacobs, Mathias Schubert, Yuhao Zhang and Marko J. Tadjer, Appl. Phys. Rev. 9, 011315 (2022).
17. Duyoung Yang, Byungsoo Kim, Tae Hoon Eom, Yongjo Park and Ho Won Jang, Electronic Materials Letters (in press), https://doi.org/10.1007/s13391-021-00333-5
18. R. Schewski, G. Wagner, M. Baldini, D. Gogova, Z. Galazka, T. Schulz, T. Remmele, T. Markurt, H. von Wenckstern, M. Grundmann, O. Bierwagen, P. Vogt, and M. Albrecht, Appl. Phys. Express 8, 011101 (2014).
19. M. Kracht, A. Karg, M. Feneberg, J. Bl€asing, J. Sch€ormann, R. Goldhahn, and M. Eickhoff, Phys. Rev. Appl. 10, 024047 (2018).
20. Y. Oshima, K. Kawara, T. Shinohe, T. Hitora, M. Kasu, and S. Fujita, APL Mater. 7, 022503 (2019).
21. K. Kawara, Y. Oshima, M. Okigawa, and T. Shinohe, Appl. Phys. Express 13, 075507 (2020).
22. A. Sharma and U. Singisetti, Appl. Phys. Lett. 118, 032101 (2021).
23. A. Segura, L. Artus, R. Cusco, R. Goldhahn, and M. Feneberg, Phys. Rev. Mater. 1, 024604 (2017).

24. M. Hilfiker, R. Korlacki, R. Jinno, Y. Cho, H. G. Xing, D. Jena, U. Kilic, M. Stokey, and M. Schubert, Appl. Phys. Lett. 118, 062103 (2021).
25. M. Feneberg, J. Nixdorf, M. D. Neumann, N. Esser, L. Artus, R. Cusco, T.Yamaguchi, and R. Goldhahn, Phys. Rev. Mater. 2, 044601 (2018).
26. M. Stokey, R. Korlacki, M. Hilfiker, S. Knight, S. Richter, V. Darakchieva, R. Jinno, Y. Cho, G. H. Xing, D. Jena, Y. Oshima, K. Khan, E. Ahmadi, and M. Schubert, Phys. Rev. Mater. 6, 014601 (2021).
27. S.I. Kan, S. Takemoto, K. Kaneko, I.Takahashi, M. Sugimoto, and T. Shinohe, Appl. Phys. Lett. 113, 212104 (2018).
28. J.G. Hao, H.H. Gong, X.H. Chen, Y. Xu, F.F. Ren, and S.L. Gu, Appl. Phys. Lett. 118, 261601 (2021).
29. [9] Alexandros Kyrtsos, Masahiko Matsubara, and Enrico Bellotti, On the feasibility of p-type Ga_2O_3, Appl. Phys. Lett. 112, 032108 (2018).
30. Peter Deak, Quoc Duy Ho, Florian Seemann, Balint Aradi, Michael Lorke, and Thomas Frauenhei, Phys. Rev. B 95, 075208 (2017).
31. Kentaro Kaneko, Yasuhisa Masuda, Shin-ichi Kan, Isao Takahashi, Yuji Kato, Takashi Shinohe, and Shizuo Fujita, Appl. Phys. Lett. 118, 102104 (2021).
32. S.I. Stepanov, V.I. Nikolaev, A.V.Almaev, A.I.Pechnikov, M.P. Scheglov, A.V. Chikiryaka, B.O. Kushnarev, A.Y. Polyakov, Materials Physics and Mechanics, 47, 577 (2021).
33. Dae-Woo Jeon, Hoki Son , Jonghee Hwang , A.Y. Polyakov, N.B. Smirnov, I.V. Shchemerov, A.V. Chernykh, A.I. Kochkova, S.J. Pearton, In-Hwan Lee, APL Materials 6, 121110 (2018).
34. T.C. Ma, X.H. Chen, Y. Kuang, L. Li, J. Li, F. Kremer, F.F. Ren, S.L. Gu, R. Zhang, Y.D. Zheng, H.H. Tan, C. Jagadish and J.D. Ye,. Appl. Phys. Lett. 115, 182101 (2019).

35. H. Son, Y.J. Choi, J.; Hwang and D.W. Jeon, ECS J. Solid State Sci. Technol. 8, Q3024 (2019).

36. A. Y. Polyakov, V. I. Nikolaev, S. I. Stepanov, A. I. Pechnikov, E. B. Yakimov, N. Smirnov, I. V. Shchemerov, A. A. Vasilev, A. I. Kochkova, A.V. Chernykh, and S. J. Pearton, ECS J. Solid State Sci. Technol, 9, 045003 (2020).

37. Capacitance spectroscopy of semiconductors, ed. Jian V. Li and Giorgio Ferrari (Pan Stanford Publishing Pte Ltd, Singapore, 2018) 437 pp

38. A. Y. Polyakov, N. B. Smirnov, I. V. Shchemerov, S. J. Pearton, Fan Ren, A. V. Chernykh, and A. I. Kochkova, Appl. Phys. Lett. 113, 142102 (2018)

39. A. Y. Polyakov, N. B. Smirnov, I. V. Shchemerov, S. J. Pearton, F. Ren, A. V. Chernykh, P. B. Lagov, and T. V. Kulevoy, APL Materials 6, 096102 (2018).

40. Rujun Sun, Yu Kee Ooi, Peter T. Dickens, Kelvin G. Lynn, and Michael A. Scarpulla, Appl. Phys. Lett. 117, 052101 (2020).

41. Cecilia Guillén and José Herrero, Electron. Mater.2, 49 (2021).

42. Zhishan Mi, Li Chen, Changmin Shi, Yan Ma, Dongchao Wang, Xiaolong Li, Hingmei Liu, Lijie Qiao, Computational Mater. Sci., 144, 64 (2018).

FIGURE CAPTIONS

Fig. 1(Color online) I-V characteristics obtained for Ti/Au Ohmic contacts on the Cr_2O_3 film at 298 K (solid black line) and 397K (solid red line), blue dashed lines show the photocurrent measured under 365 nm LED illumination.

Fig. 2 (Color online) Temperature dependence of Ohmic current through the Cr_2O_3 films.

Fig. 3 (Color online) MCL spectrum of the Cr_2O_3 films.

Fig. 4 (Color online) Room temperature C-f characteristics measured at 0V for the sample with no Cr_2O_3 underlayer (red line) and with such underlayer (blue line).

Fig. 5 (Color online) (a) Room temperature $1/C^2$ versus V plots measured for the sample with no Cr_2O_3 buffer at 300 Hz (red line) and 3 kHz (blue line); (b) the $1/C^2$ versus V plots for the sample with Cr_2O_3 buffer at 70 Hz and 1 kHz.

Fig. 6 (Color online) Plots of charge concentration versus depth calculated for the sample with no Cr_2O_3 buffer from C-V data obtained at 300 Hz (sum of shallow and deep donors) and at 3 kHz (only shallow donors).

Fig. 7(Color online) (a) 300K I-V characteristics of the sample without Cr_2O_3 buffer in the dark and under illumination with high-power LED with peak wavelength 365 nm and optical power density 25 mW/cm^2 and 250 mW/cm^2, also shown is the curve obtained with 259 nm LED (2.25 mW/cm^2 excitation); (b) 300K I-V characteristics measured for a sample with Cr_2O_3 buffer in the dark (black line) and under illumination with different LEDs; data shown for high-power (250 mW/cm^2) illumination with 660 nm (red line), 530 nm (olive line), 365 nm (orange line) and for 259 nm LED illumination with output power density 2.25 mW/cm^2 (violet line).

Fig. 8 (Color online) I-V characteristic measured at room temperature between two Ohmic Ti/Au contacts on the sample with Cr_2O_3 buffer.

Fig.9 (Color online) Photocapacitance ΔC_{ph} (the difference between the capacitance under illumination and in the dark, C_{dark}) normalized by C_{dark} for the sample with no Cr_2O_3 buffer (red

line, open squares) and with Cr_2O_3 buffer (blue line, solid squares); the data shown for excitation with LEDs with wavelengths from 940-365 nm and same optical power output of 250 W/cm^2.

Fig. 10 (Color online) (a) Photocurrent density at -4V (dark current density subtracted) spectra for the sample with no Cr_2O_3 buffer; (b) the same for forward and reverse bias for sample with Cr_2O_3 buffer.

Fig. 11 (Color online) PICTS spectra measured at -1V with 365 nm LED excitation, for time windows 60 ms/6000 ms and pulse length 5s for the sample with no Cr_2O_3 buffer (red line) and with Cr_2O_3 buffer (red line).

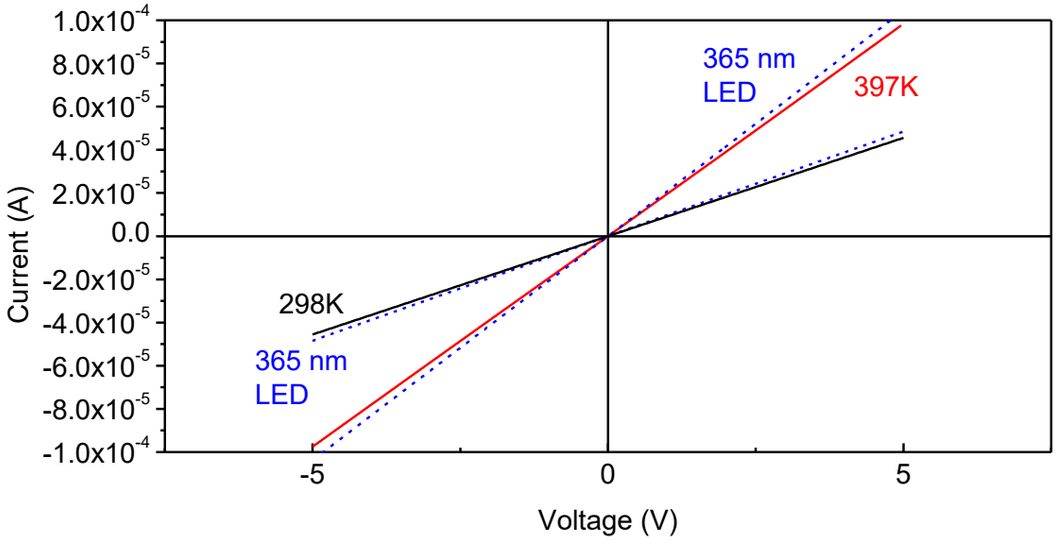

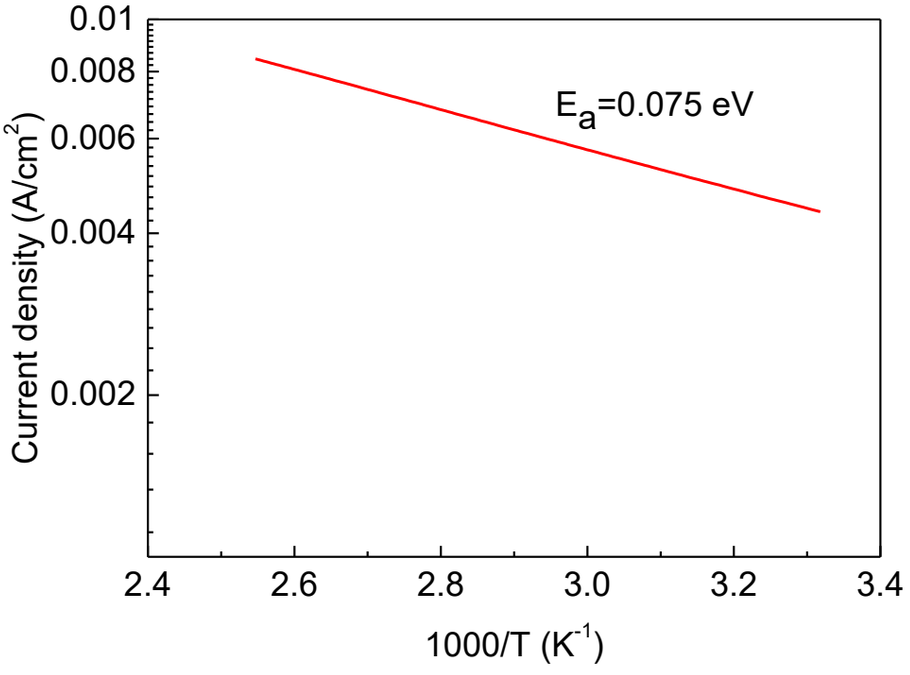

AIP Publishing
Journal of Applied Physics
ACCEPTED MANUSCRIPT

PLEASE CITE THIS ARTICLE AS DOI: 10.1063/5.0090832

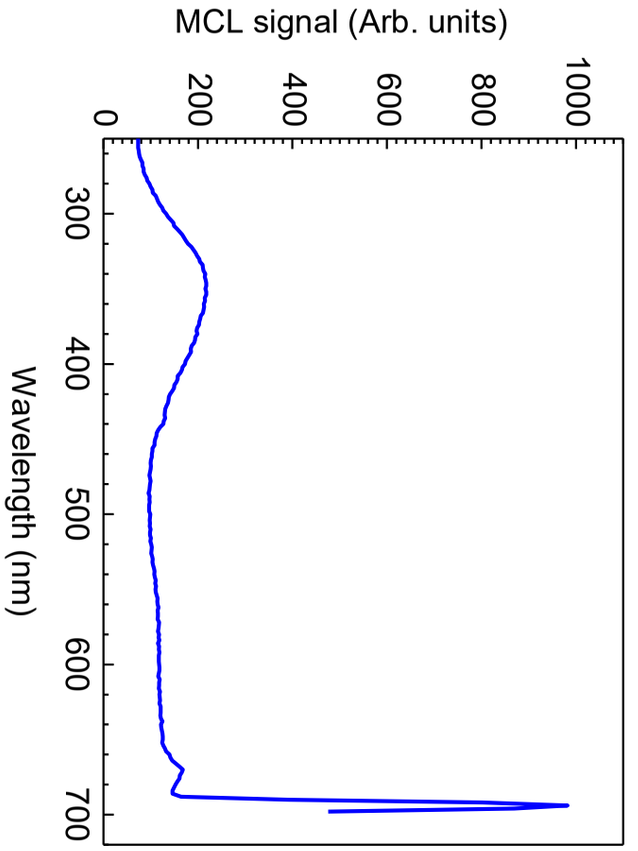

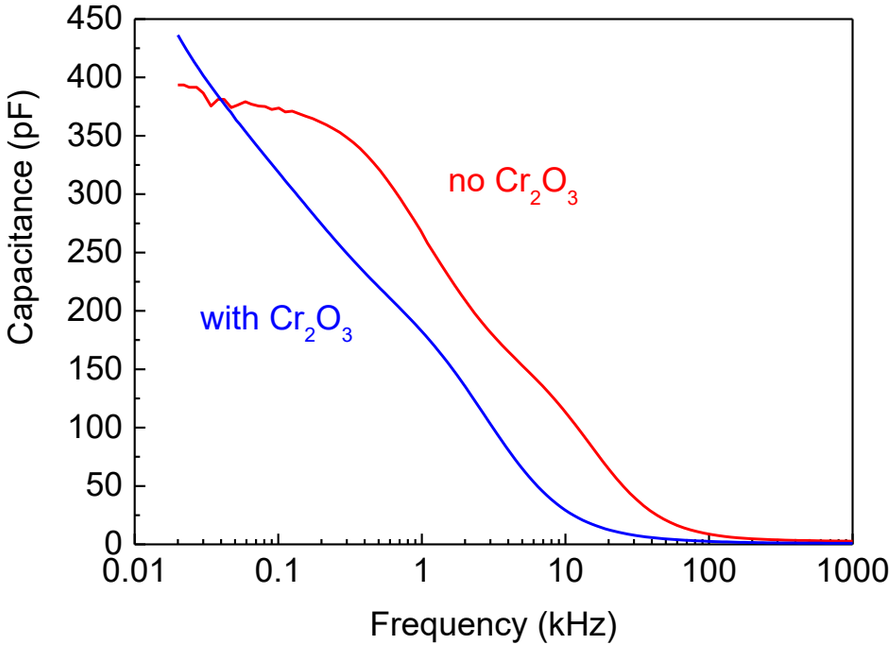

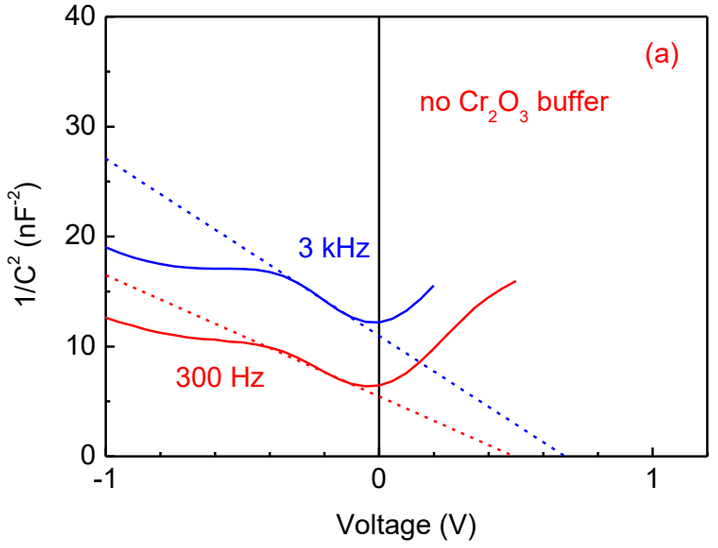

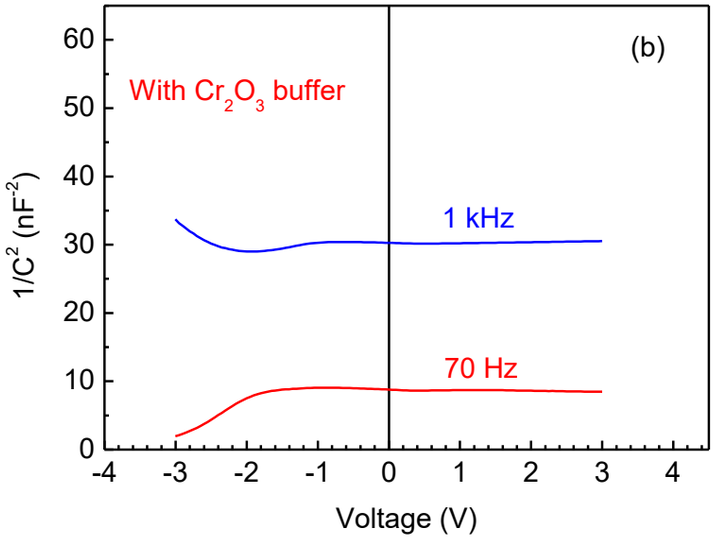

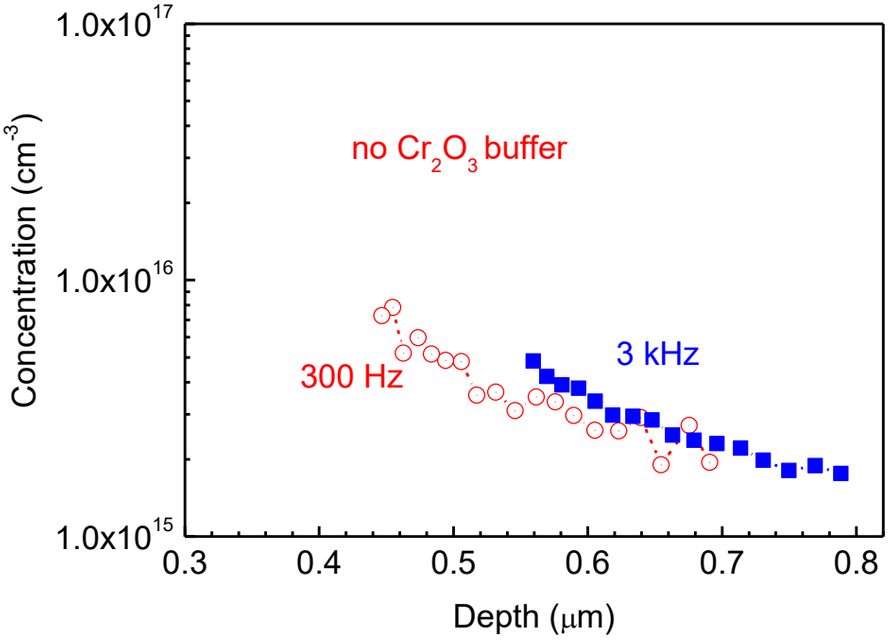

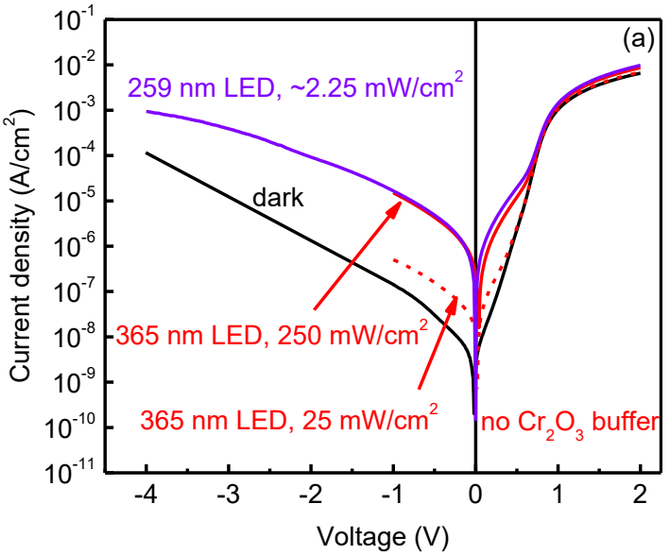

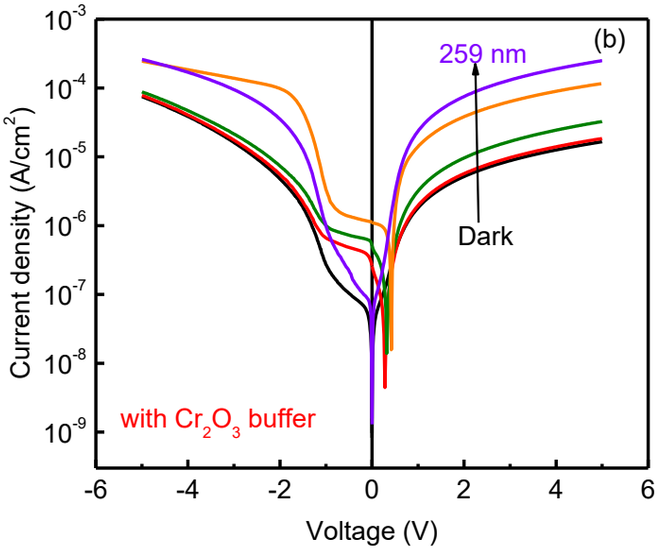

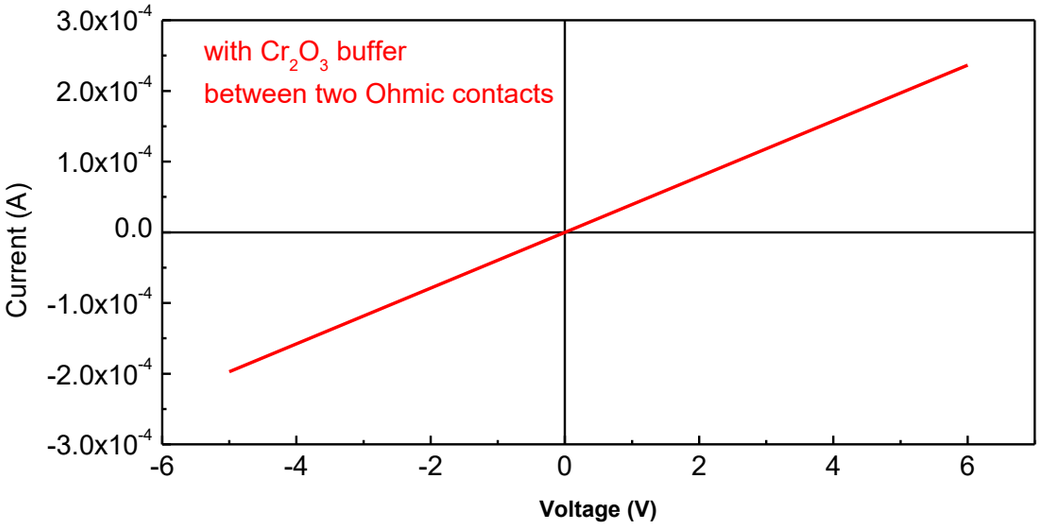

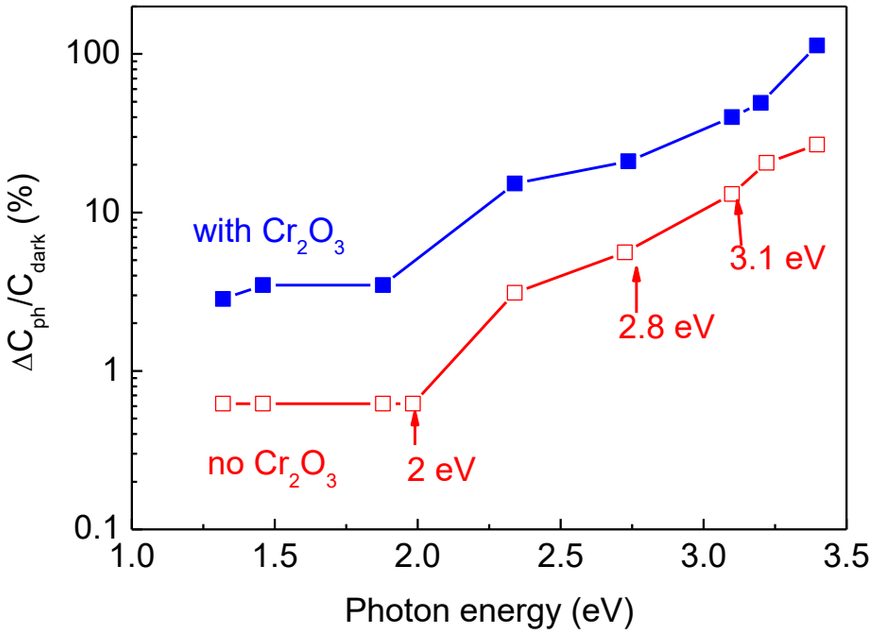

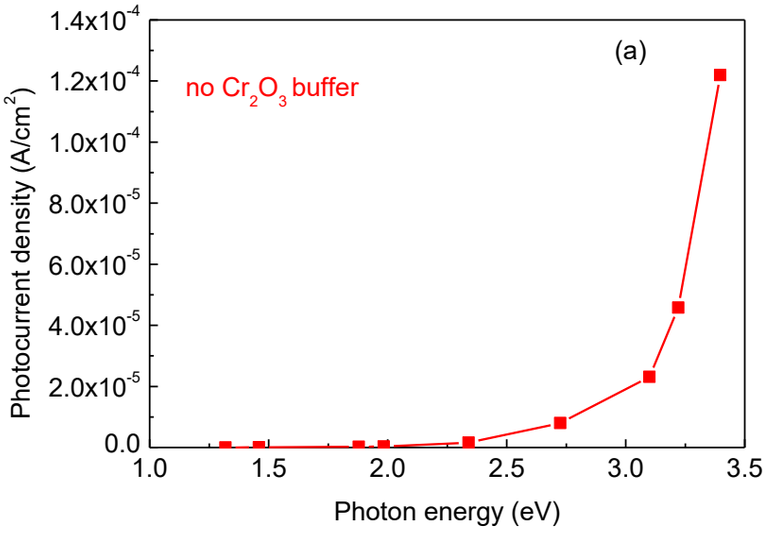

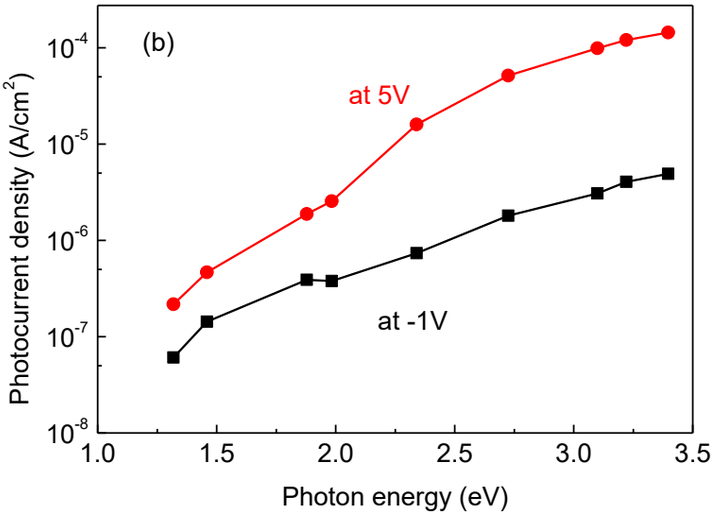

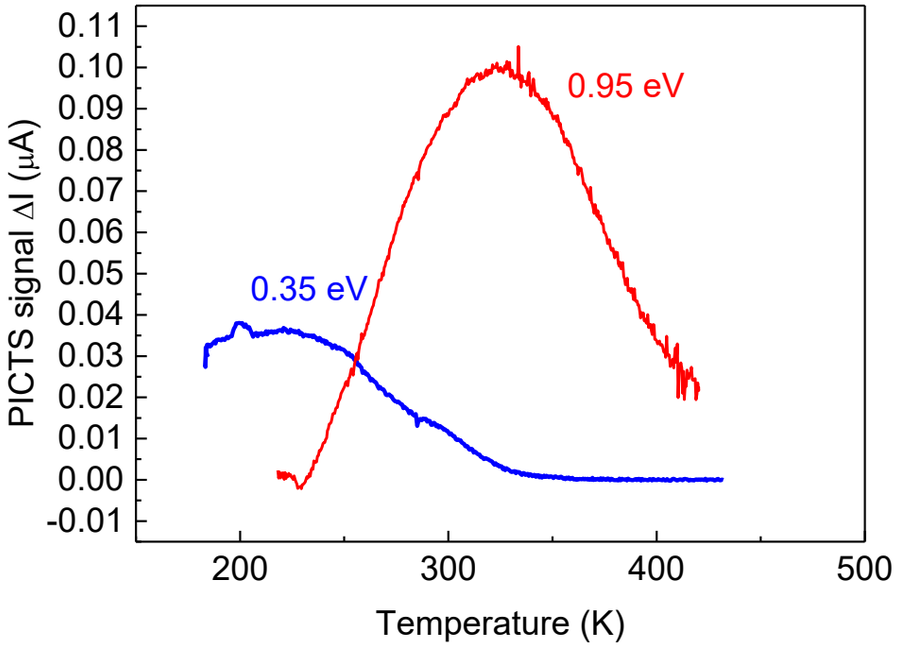

AIP Publishing

Journal of Applied Physics

ACCEPTED MANUSCRIPT

This is the author's peer reviewed, accepted manuscript. However, the online version of record will be different from this version once it has been copyedited and typeset.
PLEASE CITE THIS ARTICLE AS DOI: 10.1063/5.0090832

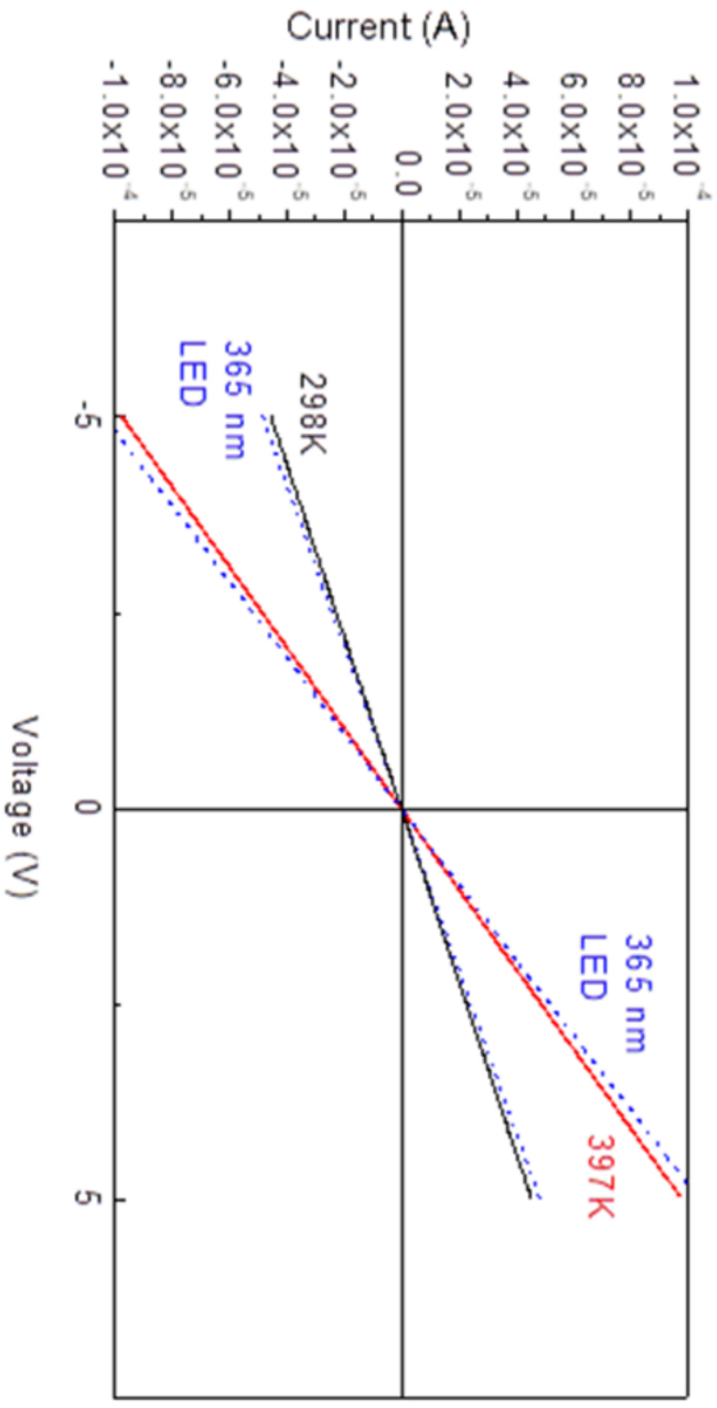

AIP Publishing

Journal of Applied Physics

ACCEPTED MANUSCRIPT

This is the author's peer reviewed, accepted manuscript. However, the online version of record will be different from this version once it has been copyedited and typeset.
PLEASE CITE THIS ARTICLE AS DOI: 10.1063/5.0090832

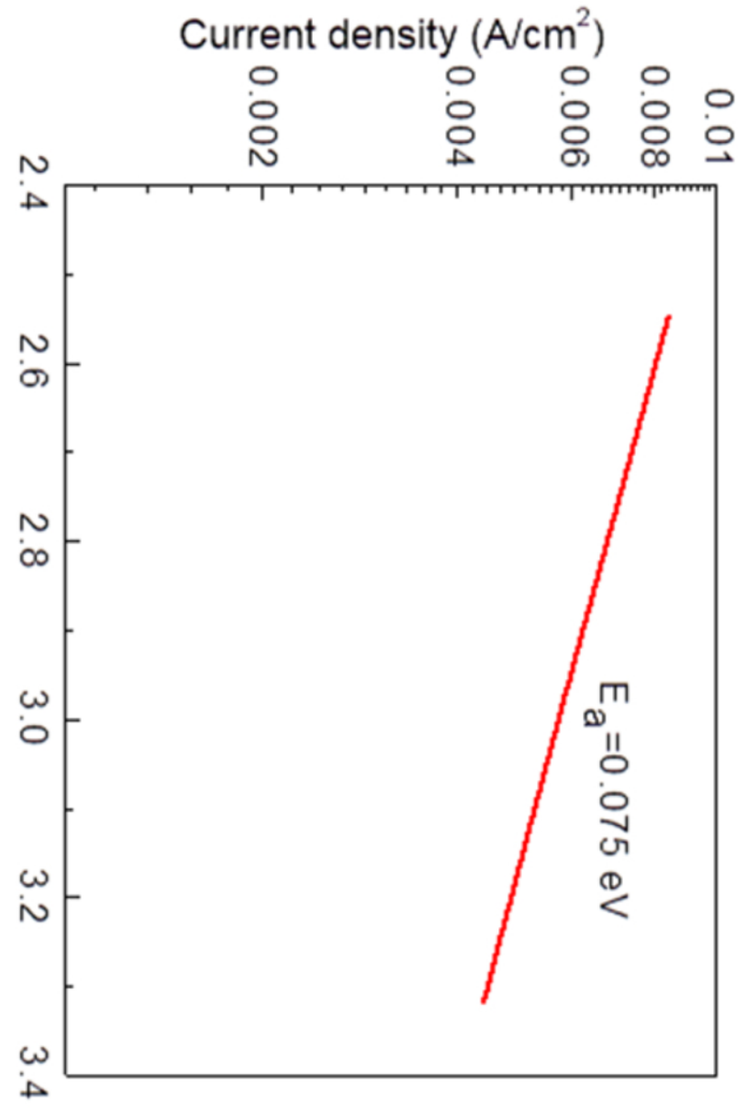

Journal of Applied Physics

PLEASE CITE THIS ARTICLE AS DOI: 10.1063/5.0090832

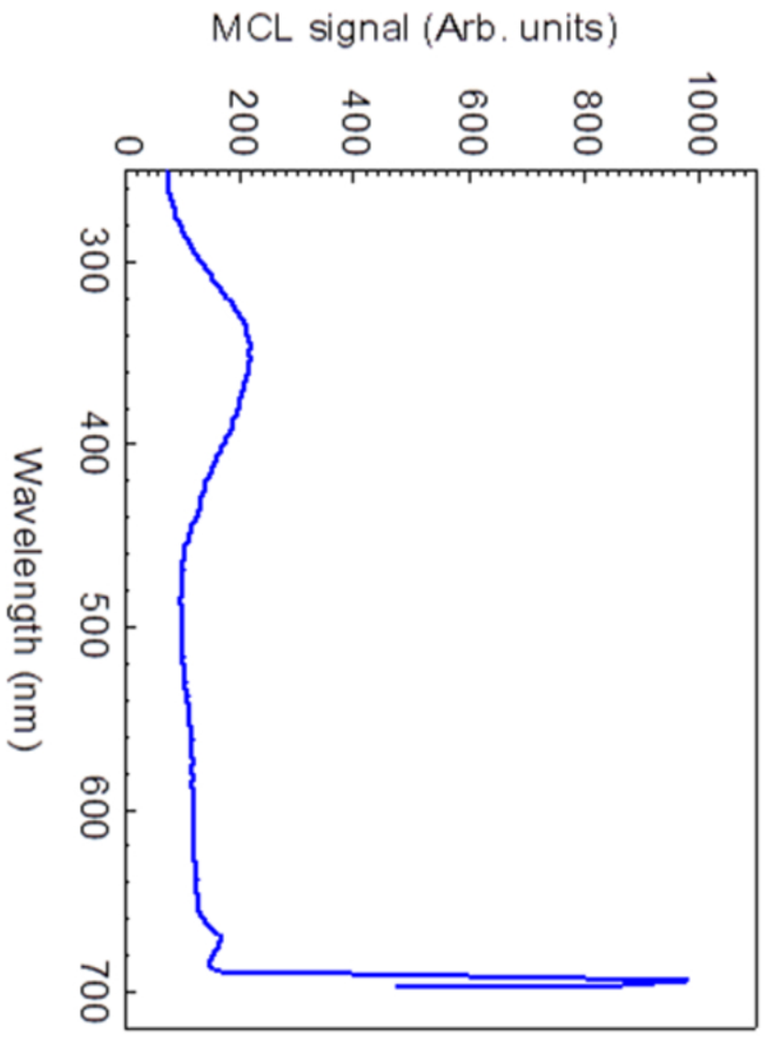

Journal of Applied Physics

PLEASE CITE THIS ARTICLE AS DOI: 10.1063/5.0090832

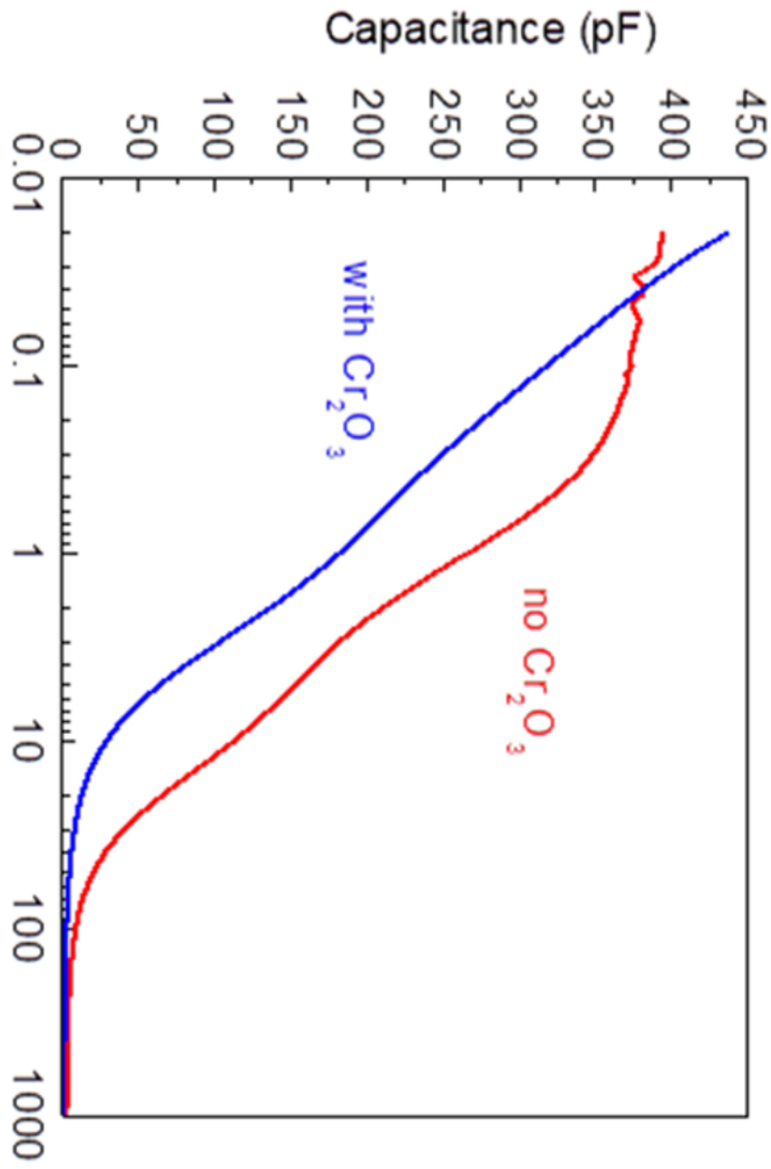

Journal of Applied Physics

PLEASE CITE THIS ARTICLE AS DOI: 10.1063/5.0090832

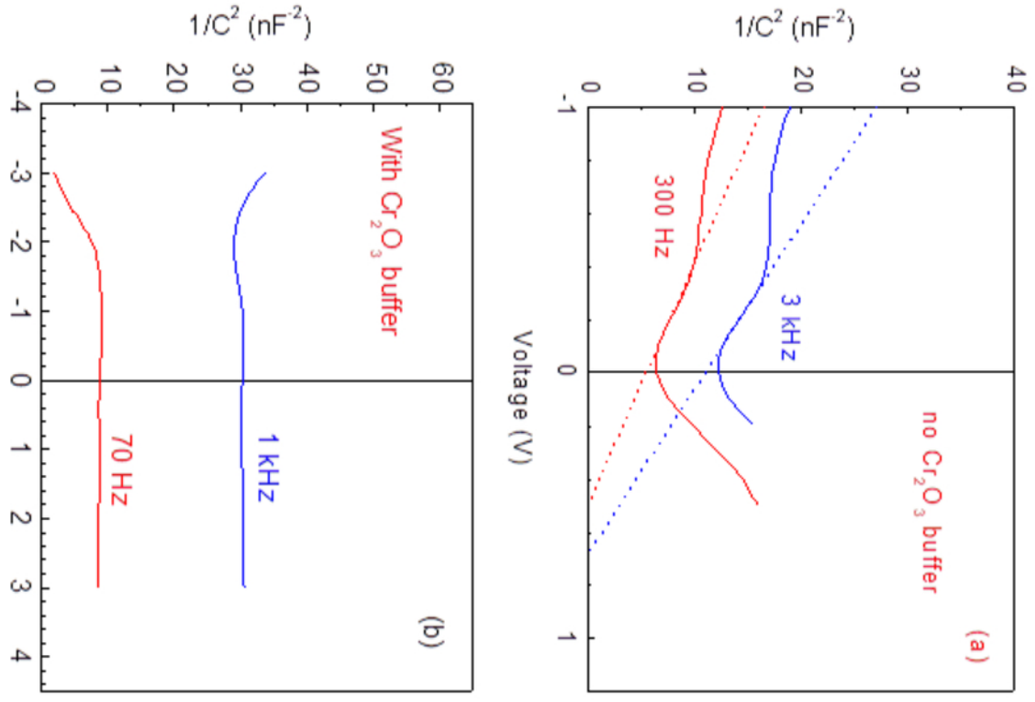

Journal of Applied Physics

PLEASE CITE THIS ARTICLE AS DOI: 10.1063/5.0090832

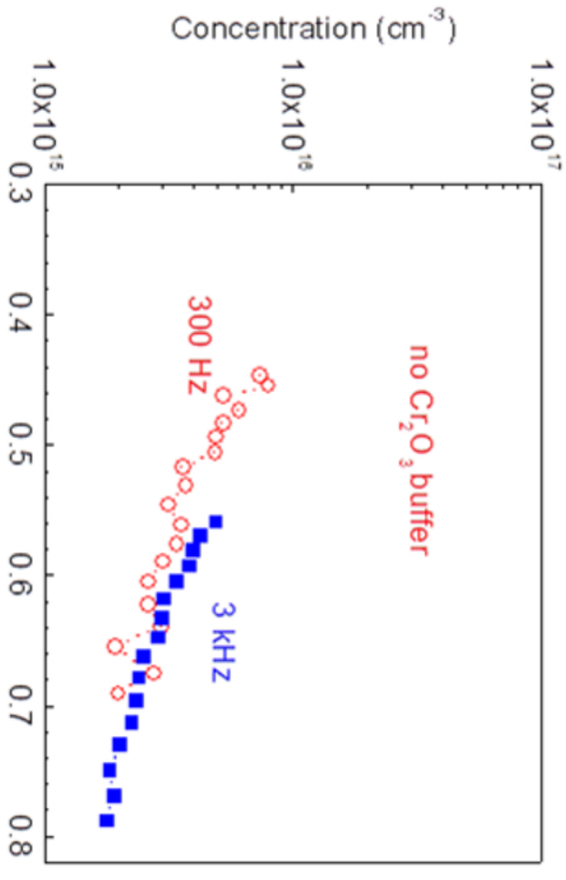

Journal of Applied Physics

PLEASE CITE THIS ARTICLE AS DOI: 10.1063/5.0090832

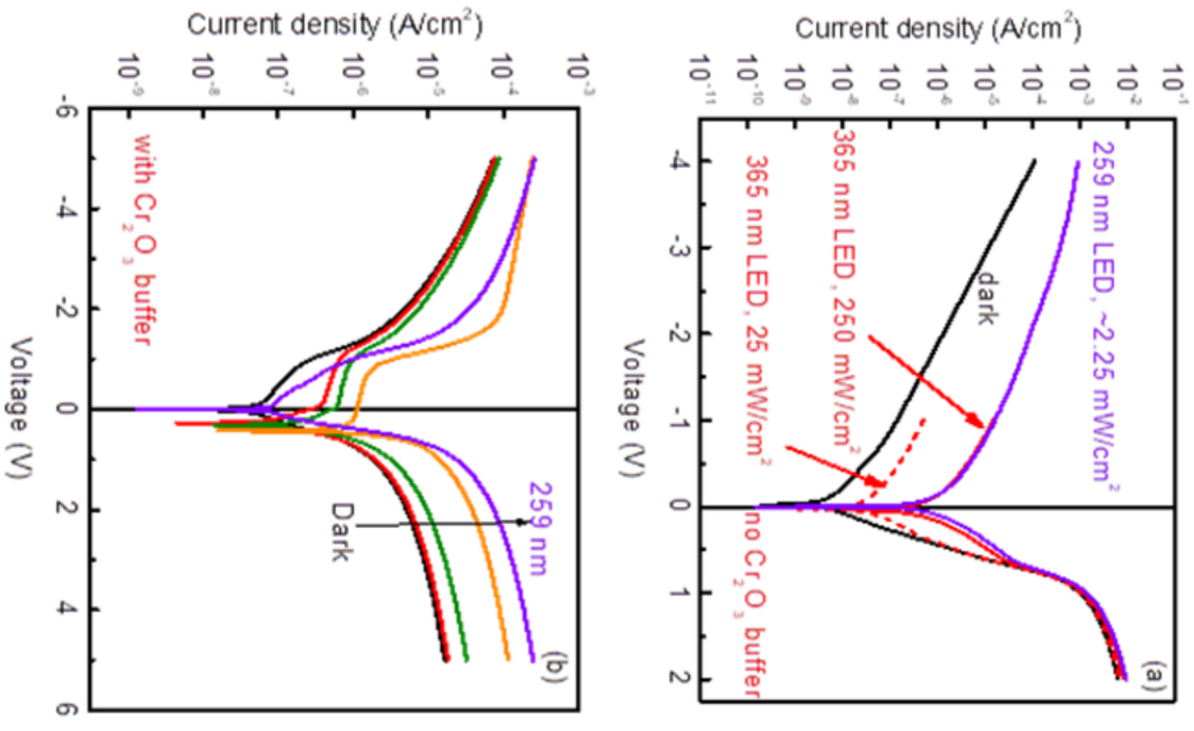

AIP Publishing

Journal of Applied Physics

ACCEPTED MANUSCRIPT

This is the author's peer reviewed, accepted manuscript. However, the online version of record will be different from this version once it has been copyedited and typeset.
PLEASE CITE THIS ARTICLE AS DOI: 10.1063/5.0090832

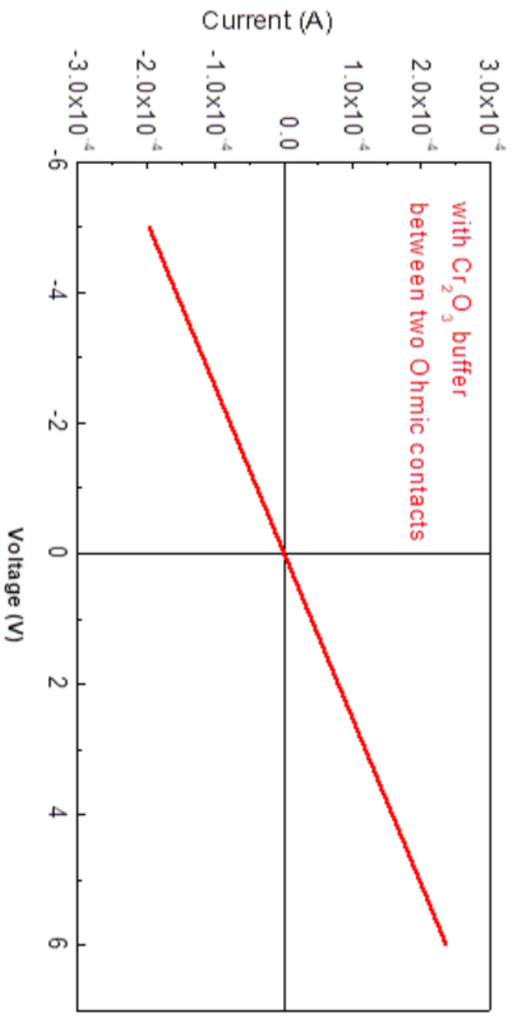

Journal of Applied Physics

PLEASE CITE THIS ARTICLE AS DOI: 10.1063/5.0090832

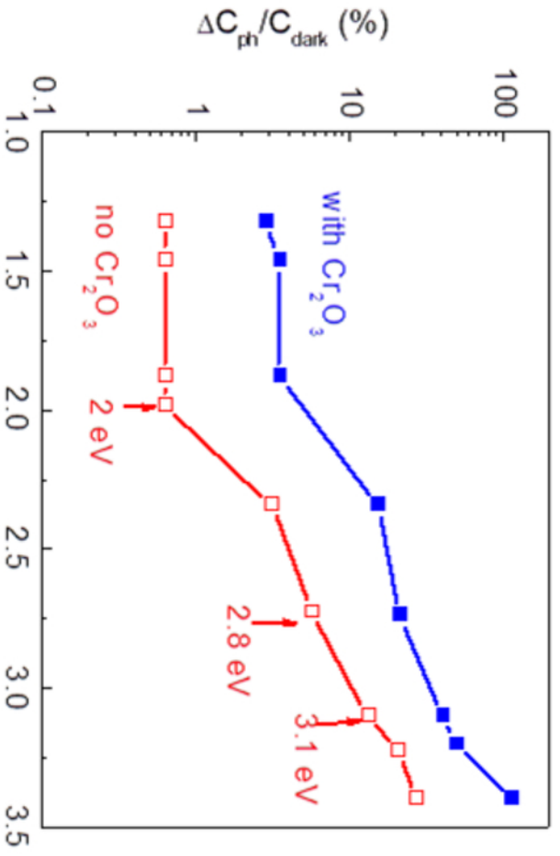

AIP Publishing

Journal of Applied Physics

ACCEPTED MANUSCRIPT

This is the author's peer reviewed, accepted manuscript. However, the online version of record will be different from this version once it has been copyedited and typeset.
PLEASE CITE THIS ARTICLE AS DOI: 10.1063/5.0090832

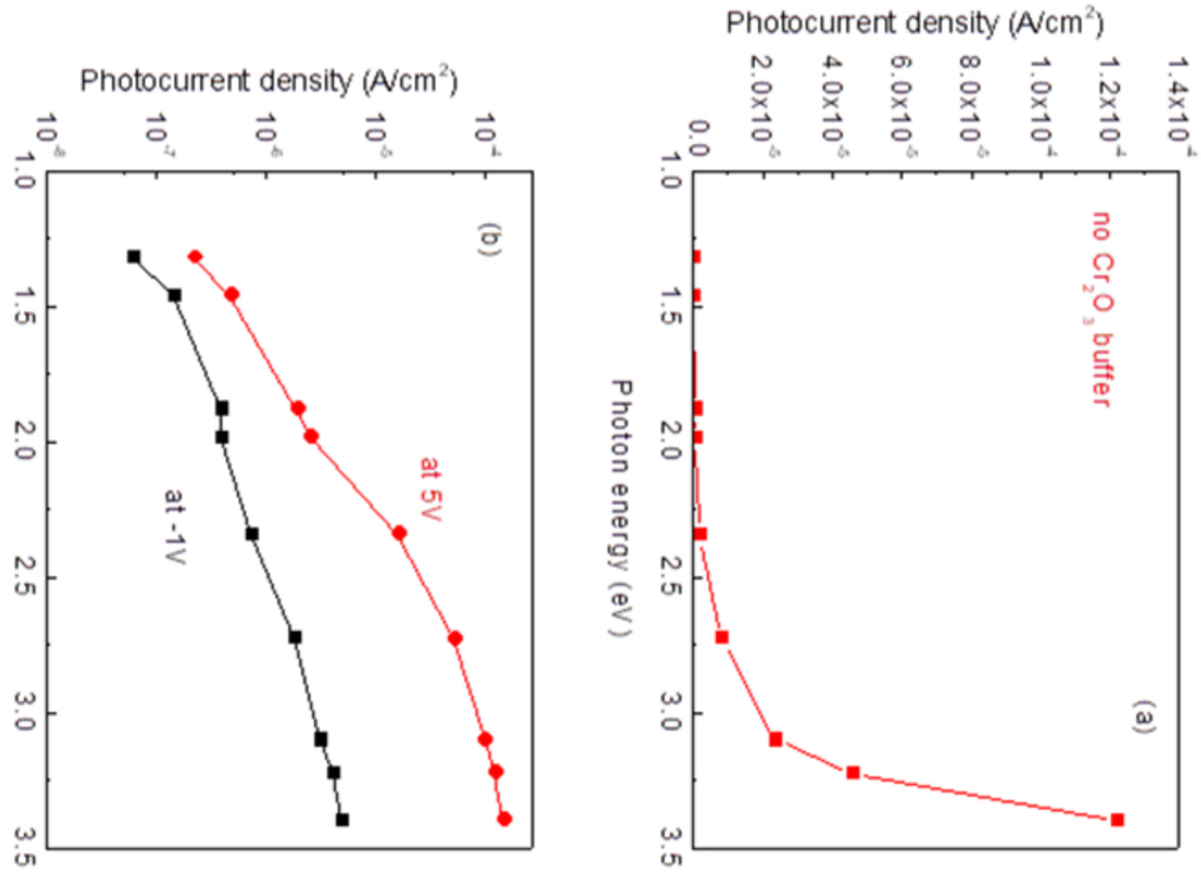

Journal of Applied Physics

PLEASE CITE THIS ARTICLE AS DOI: 10.1063/5.0090832